Applied Catalysis B: Environmental 218 (2017) 230–239

Contents lists available at ScienceDirect

Applied Catalysis B: Environmental

journal homepage: www.elsevier.com/locate/apcatb

Visible-light-assisted peroxymonosulfate activation and mechanism for the degradation of pharmaceuticals over pyridyl-functionalized graphitic carbon nitride coordinated with iron phthalocyanine

Fei Wu, Huawang Huang, Tiefeng Xu, Wangyang Lu*, Nan Li, Wenxing Chen*

National Engineering Lab for Textile Fiber Materials & Processing Technology (Zhejiang), Zhejiang Sci-Tech University, Hangzhou 310018, China

ARTICLE INFO

Article history:
Received 23 March 2017
Received in revised form 30 May 2017
Accepted 19 June 2017
Available online 20 June 2017

Keywords:
$g\text{-}C_3N_4$
Excited-state $FePcCl_{16}$
Visible light
Mechanism
Degradation pathway

ABSTRACT

Recently, peroxymonosulfate (PMS)-based advanced oxidation processes (AOPs) have received increasing attention because of their capability and adaptability in decontamination. The couple of solar light and PMS activation is an environmentally friendly and efficient strategy for environmental remediation. Herein, the iron hexadecachlorophthalocyanine ($FePcCl_{16}$) was used to coordinate with graphitic carbon nitride ($g\text{-}C_3N_4$), which was functionalized by pyridine-based ligand isonicotinic acid (INA) to prepare a distinctive catalyst, $g\text{-}C_3N_4$-INA-$FePcCl_{16}$. The experimental results revealed that $g\text{-}C_3N_4$-INA-$FePcCl_{16}$ can activate PMS efficiently for the elimination of carbamazepine (CBZ) under visible light irradiation over a wide pH range. Upon irradiation with visible light, CBZ was destroyed by the solider $g\text{-}C_3N_4$ with generated sulfate ($SO_4^{\bullet-}$) and hydroxyl ($^{\bullet}OH$) radicals, on the other hand, high-valent iron (Fe (IV) = O) species accompanied by $SO_4^{\bullet-}$ and $^{\bullet}OH$ radicals were produced by excited-state $FePcCl_{16}$ ($^{*}FePcCl_{16}$) during oxidation, which is different from a traditional PMS activation system. The axial pyridine-based ligand was protected under the $FePcCl_{16}$ macrocyclic structure shield. Noteworthy, in the absence of visible light, $g\text{-}C_3N_4$-INA-$FePcCl_{16}$ showed a higher catalytic performance than pure $g\text{-}C_3N_4$, $FePcCl_{16}$ and a mechanical mixture of the two. This study allows for the construction of an effective and environmental catalytic system, which can be applied to purify water that contains refractory pollutants.

1. Introduction

The occurrence of pharmaceutically active compounds (PhACs) in environments has received increasing attention because of their potential threat to human health and aquatic ecosystems [1,2]. As emerging persistent contaminants, PhACs are believed to be toxic to living organisms even though the concentration is very low [3]. Therefore, it is necessary to develop efficient technologies to eliminate PhACs. Advanced oxidation processes (AOPs) that use reactive species have been applied extensively in rapid degradation and complete mineralization of the recalcitrant organic pollutants [4–6]. Among various AOPs, peroxymonosulfate (PMS, $2KHSO_5{\cdot}KHSO_4{\cdot}K_2SO_4$, oxone), as a favorable alternative to hydrogen peroxide (H_2O_2), has received attention because of its ability to generate both hydroxyl ($^{\bullet}OH$) and sulfate ($SO_4^{\bullet-}$) radicals, as well as its improved flexibility over a broad pH range [7,8]. Numerous methods for PMS activation have been proposed including transition metals [9–12], ultraviolet (UV) [13], ultrasound [14], carbon catalysts [15,16] and so on. The most common catalysts are transition metals, with Co^{2+}/PMS system gives the best results of $SO_4^{\bullet-}$ generation. However, the application of Co^{2+} is limited because of its potential carcinogenic effects [17].

In contrast with cobalt, iron is more environmentally friendly, which makes it a potentially fascinating catalyst. Recently, some investigations have reported the use of Fe^{2+} in PMS activation to form active radical species [18,19]. However, the Fe^{2+}/PMS system can only be operated under acidic conditions because of the hydrolysis and precipitation of Fe^{2+} [20], and the transformation rate from Fe^{3+} to Fe^{2+} is slow [21,22]. Iron phthalocyanine (FePc) is a potential material that could overcome these drawbacks. FePc as an efficient and stable Fenton-like catalyst could improve the pH tolerance for a higher catalytic performance [23]. It may be also applicable to PMS-related conditions. Second, the unique electron-rich characteristic of FePc could accelerate the transformation rate from Fe^{3+} to Fe^{2+} [24]. Simultaneously, FePc is a member of the metallophthalocyanines (MPcs) family, which is well-known for an intrinsic broad spectral response in the red/near-infrared (IR) and visible-light region, and has been applied widely in the photocatalytic field

* Corresponding authors.
E-mail addresses: luwy@zstu.edu.cn (W. Lu), wxchen@zstu.edu.cn (W. Chen).

http://dx.doi.org/10.1016/j.apcatb.2017.06.057
0926-3373/

[25–27]. Accompanied by light-harvesting, MPcs can be excited to their excited state with unique photochemical and photophysical behaviors, many studies related to excited-state MPcs have been reported [28–30]. So far, numerous derivatives of FePc have been synthesized with various substituent groups [24,31–33]. Among them, iron hexadecachlorophthalocyanine ($FePcCl_{16}$) is considered more stable because the strong electron-withdrawing chlorinated substituents at the periphery can protect its macrocyclic structure. However, the use of $FePcCl_{16}$ is limited because of its aggregation, which can be overcome by introducing appropriate support materials.

In recent years, graphitic carbon nitride (g-C_3N_4) as a visible-light photocatalyst has been used widely because of its unique planar structure, photocatalysis, low cost, and thermal stability [34–37]. More recently, g-C_3N_4 has been found to be a feasible candidate for the catalytic activation of PMS towards the degradation of organic contaminants [38–40]. However, the rapid charge recombination, low surface and poor absorption of visible light have restricted its application. Many strategies have been explored to enhance its photocatalytic activity, such as heteroatom doping [41,42], heterojunctions construction [43,44] and dye sensitizing [45]. We noted that the immobilization of MPcs onto g-C_3N_4 could extend the spectral response region of g-C_3N_4, improve the MPcs dispersion and provide them with specific photoelectronic properties [25,46,47]. In our previous study, we prepared g-C_3N_4/ZnTcPc catalyst using g-C_3N_4 coupled with zinc tetracarboxyphthalocyanine (ZnTcPc), and the product showed a higher photocatalytic activity [48]. But the preparation method for this catalyst is only suitable for MPcs with carboxyl, which are difficult to obtain. Inspired by MPcs can be linked covalently or noncovalently to other ligands, such as porphyrin, pyridine, and indole, which can also be fixed to g-C_3N_4. So, an appropriate ligand was proposed as a "bridge" to connect various MPcs and g-C_3N_4.

In this work, we used pyridine-based ligand isonicotinic acid (INA) to act as a "bridge", and designed a facile approach to synthesize a distinctive catalyst, g-C_3N_4-INA-$FePcCl_{16}$, using $FePcCl_{16}$ that is axially coordinated with INA-modified g-C_3N_4. Carbamazepine (CBZ), is one of the most frequently detected PhACs in the aquatic environment, and was selected as probe compound to evaluate the catalytic performance of the as-prepared catalysts. The constructed g-C_3N_4-INA-$FePcCl_{16}$/PMS/visible light system shows strong catalytic activity for CBZ decomposition, which is attributed to the efficient generation of Fe (IV) = O, $SO_4^{\bullet-}$ and •OH. And visible-light-induced $^*FePcCl_{16}$ was identified as the major factor that is responsible for the formation of Fe (IV) = O species, which could not be detected in the dark. A possible pathway for the degradation of CBZ was proposed using high-definition mass spectrometry (HDMS) coupled with gas chromatography/mass spectrometry (GC–MS).

2. Experimental

2.1. Materials and reagents

CBZ, benzotriazol-1-yl-oxytripyrrolidinophosphonium hexafluorophosphate (PyBOP), PMS, diisopropylethylamine (DIEA) and dimethyl sulfone ($DMSO_2$) were from Aladdin Chemical Co. Ltd. Tetrahydrifuran (THF) and dimethyl sulfoxide (DMSO) were from the Tianjin Wing Tai Chemical Co. Ltd. 5, 5-Dimethyl-pyrroline N-oxide (DMPO) was obtained from the Tokyo Chemical Industry Co. Ltd. Methanol and acetonitrile (Merck, Germany) for UPLC were of chromatographic grade. All chemicals were of analytical grade and were used as received without further purification.

2.2. Catalyst preparation

g-C_3N_4 synthesis was according to Chen et al. [49]. $FePcCl_{16}$ was synthesized according to the literature [50]. The preparation of g-C_3N_4-INA-$FePcCl_{16}$ is as shown in Scheme 1. An environmental liquid exfoliation route was conducted by exfoliating g-C_3N_4 into ultrathin nanosheets in ultrapure water for 5 d, before it was freeze-dried for further use [51]. INA, PyBOP and DIEA were dissolved in 200 mL dry DMF, and ultrasonicated for 1.5 h. The ultrasonicated g-C_3N_4 was dispersed in 100 mL dry DMF and added drop-wise to the above solution at 100 mL/h. After reacting for 6 h at 60 °C, the solution was centrifuged, washed with DMF and ultrapure water, and freeze-dried to obtain g-C_3N_4-INA powder. Finally, g-C_3N_4-INA and $FePcCl_{16}$ were added to 200 mL THF in the dark for 6 h. After reaction, the solution was centrifuged, and washed with THF and ultrapure water. Then g-C_3N_4-INA-$FePcCl_{16}$ powder was obtained after the sample was freeze-dried. A series of g-C_3N_4-INA-$FePcCl_{16}$ catalysts with diverse loading of $FePcCl_{16}$ were prepared. From the X-ray fluorescence (XRF) test, the as-prepared catalysts were defined as g-C_3N_4-INA-$FePcCl_{16}$ (0.67%), g-C_3N_4-INA-$FePcCl_{16}$ (1.70%) and g-C_3N_4-INA-$FePcCl_{16}$ (3.58%). The mechanical mixture of g-C_3N_4 and $FePcCl_{16}$ was termed g-C_3N_4/$FePcCl_{16}$ (1.70% $FePcCl_{16}$ in the mixture).

2.3. Photocatalytic experiments

To evaluate the photocatalytic activity of g-C_3N_4-INA-$FePcCl_{16}$, a Q-Sun Xe-1 test chamber (USA) (Fig. S1) served as the light source, and a UV cutoff filter (Shanghai Seagull Colored Optical Glass Co., Ltd.) was used to filter the UV light ($\lambda < 420$ nm) to ensure illumination by visible light only. CBZ was selected as a probe compound. The experiment was conducted in a 40 mL glass beaker at room temperature. Before irradiation, g-C_3N_4-INA-$FePcCl_{16}$ (0.1 g/L) was dispersed in CBZ aqueous solution (25 μM) and ultrasonicated for 2 min. PMS, was added as an oxidant. The CBZ concentration was detected by UPLC equipped with the Acquity BEH C18 column (1.7 um, 2.1 × 50 mm, Waters), and a mixture of acetonitrile and water (20:80, v/v) was used as the mobile phase with a flow rate of 0.35 mL/min for the UPLC experiments.

2.4. Analytical methods

The catalyst chemical structures were analyzed by X-ray diffraction (XRD), X-ray photoelectron spectroscopy (XPS) and Fourier transform infrared spectroscopy (FTIR). UV–vis spectra and UV–vis diffuse reflectance absorption spectra (DRS) were obtained to explore the optical absorption performance of the samples. Photoluminescence (PL) spectra and the transient photocurrent response were used to investigate the photoelectrochemical properties of the catalysts. Electron paramagnetic resonance (EPR) signals of radicals trapped by DMPO were detected in a Bruker A300 spectrometer at ambient temperature. To detect whether high-valent iron (Fe (IV) = O) species were generated, designed measurements were carried out by gas chromatography/mass spectrometry (GC–MS, GC: Agilent 6890 N equipped with an OV1701 capillary column 30 m × 0.25 mm × 0.25 um; MS: Agilent 5973i) and UPLC/Synapt G2-S HDMS (Waters Q-TOF, USA) in positive mode. The degradation intermediates of CBZ in the g-C_3N_4-INA-$FePcCl_{16}$/PMS/visible light system were identified by UPLC Synapt G2-S HDMS (Waters, USA). The procedures and corresponding parameters are described in the supplementary material.

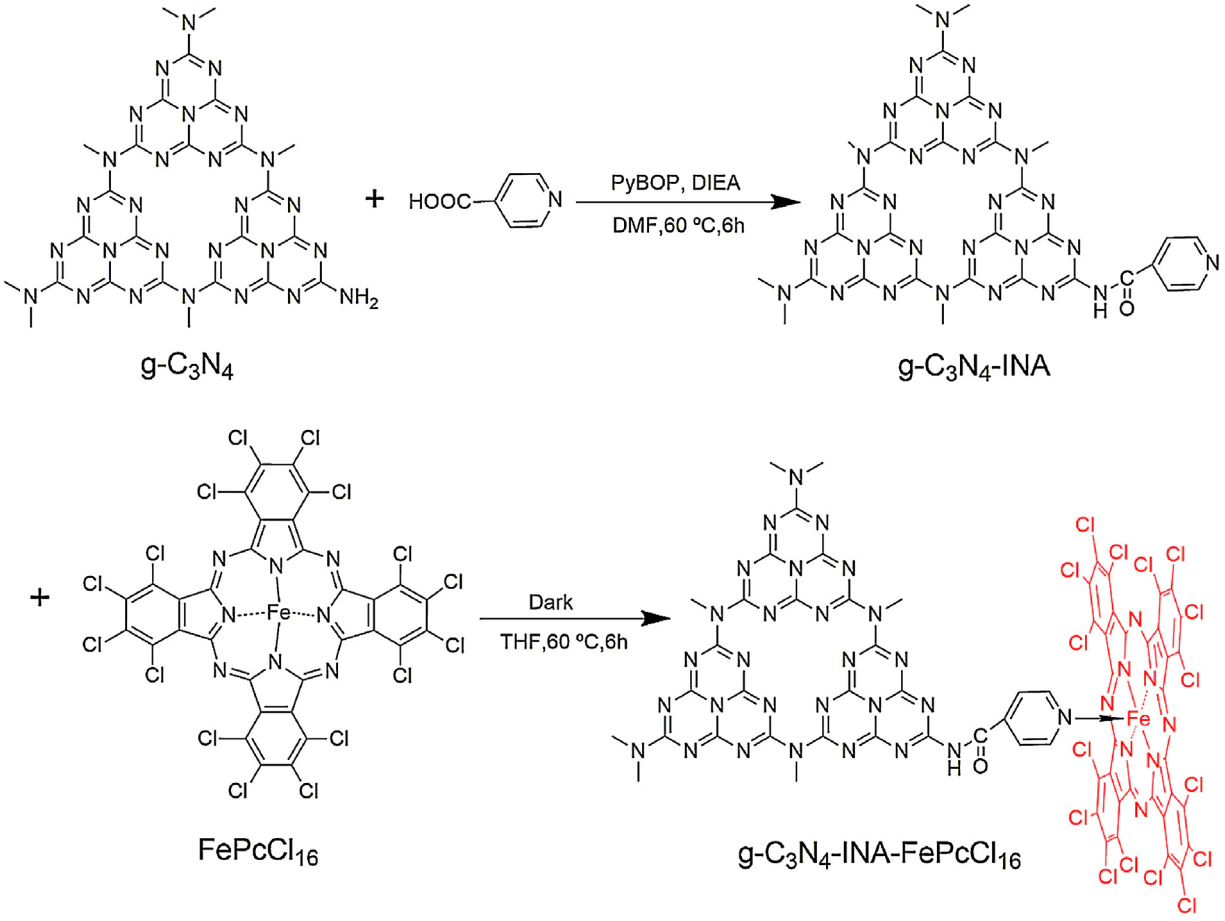

Scheme 1. Synthesis of g-C_3N_4-INA-$FePcCl_{16}$.

3. Results and discussion

3.1. Characterization

Fig. 1a shows the UV–vis absorption spectra of $FePcCl_{16}$ and the simple mixture of $FePcCl_{16}$ and INA in THF solution. $FePcCl_{16}$ solution exhibited an outstanding visible/near-IR responsive property with an intense absorption band centered at 683 nm, which favored visible-light-assisted photocatalytic contaminant decomposition. In contrast, the maximum absorption of the mixture of $FePcCl_{16}$ and INA was blue-shifted by ~4 nm, which may have resulted from the coordination interaction between INA and $FePcCl_{16}$. DRS spectra of the pure g-C_3N_4, g-C_3N_4-INA and g-C_3N_4-INA-$FePcCl_{16}$ are shown in Fig. 1b. g-C_3N_4 absorption limited visible light below 450 nm because of its relatively large bandgap (2.7 eV) [52], whereas g-C_3N_4-INA-$FePcCl_{16}$ exhibited a much broader absorption band over the entire visible light region. On the basis of the above results, we infer that the combination of g-C_3N_4-INA and $FePcCl_{16}$ induces a synergetic effect and improves the photocatalytic activity of g-C_3N_4 and $FePcCl_{16}$.

A HDMS technique was used to confirm that the INA can coordinate with $FePcCl_{16}$. Fig. 2a shows the chemical molecular structure of INA-$FePcCl_{16}$, which was formed by INA and $FePcCl_{16}$ via axial coordination. Fig. 2b shows the theoretical mass spectrum of INA-$FePcCl_{16}$, which was obtained by inputting its molecular formula ($C_{38}H_5N_9O_2Cl_{16}Fe$) into Micromass MassLynx software. Fig. 2c shows the actual mass spectrum for a simple mixture of INA and $FePcCl_{16}$ dispersed in THF solution. The fragmentation peaks of the former well coincide with the peaks of the latter, which indicates that the INA could coordinate with the $FePcCl_{16}$.

We used XPS spectra to identify the chemical composition and bonding of the g-C_3N_4, g-C_3N_4-INA-$FePcCl_{16}$ and $FePcCl_{16}$. As shown in Fig. 3, the C 1s peaks at 284.6 eV and 286.3 eV correspond to sp^2 C—C bonds and C—NH_2 species, respectively [53]. The C 1s peaks at 288.2–288.5 eV are ascribed to the C—N—C coordination and sp^2-hybridized carbon of the N—C=N [54]. For $FePcCl_{16}$, the C 1s peak at 285.9 eV is likely to be attributed to C—Cl species. We could observe that the N—C=N peak of g-C_3N_4-INA-$FePcCl_{16}$ decreased compared with the C—C peak. This may resulted from the amidation reaction between g-C_3N_4 and INA, which resulted in a decrease of the amount of N—C=N bonds. The N 1s spectra are shown in Fig. S2. The strongest peak at 398.6 eV can be explained by the sp^2-hybridized nitrogen in triazine rings (C—N=C) [55,56]. Compared with g-C_3N_4, g-C_3N_4-INA-$FePcCl_{16}$ showed a distinct increase at peak 401.0 eV, which is regarded as the nitrogen involved in amide group (—NH—CO—) that is formed by the amino (—NH_2) of g-C_3N_4 and the carboxyl (—COOH) of INA. Therefore, we have proven the specific synthesis process of g-C_3N_4-INA-$FePcCl_{16}$, which is based on axial coordination of INA-functionalized g-C_3N_4 and $FePcCl_{16}$.

XRD patterns of the different samples are given in Fig. 4. Two sharp diffraction peaks at 13.1° and 27.5° were observed in the XRD patterns for pure g-C_3N_4, g-C_3N_4-INA and g-C_3N_4-INA-$FePcCl_{16}$. The stronger peak at 27.5° can be indexed as (002) diffraction for graphitic-like structure. Another peak at 13.1° that corresponds to tristriazine units is ascribed to the (100) inplanar in JCPDS 87-1526 with an interplanar distance of 0.682 nm [57]. The results illustrate that g-C_3N_4-INA-$FePcCl_{16}$ retained the intrinsic structure of g-C_3N_4. Moreover, no diffraction peaks of the $FePcCl_{16}$ crystal appeared in the XRD pattern of g-C_3N_4-INA-$FePcCl_{16}$, which indicates the low amount and high dispersity of $FePcCl_{16}$ on g-C_3N_4 surfaces. In

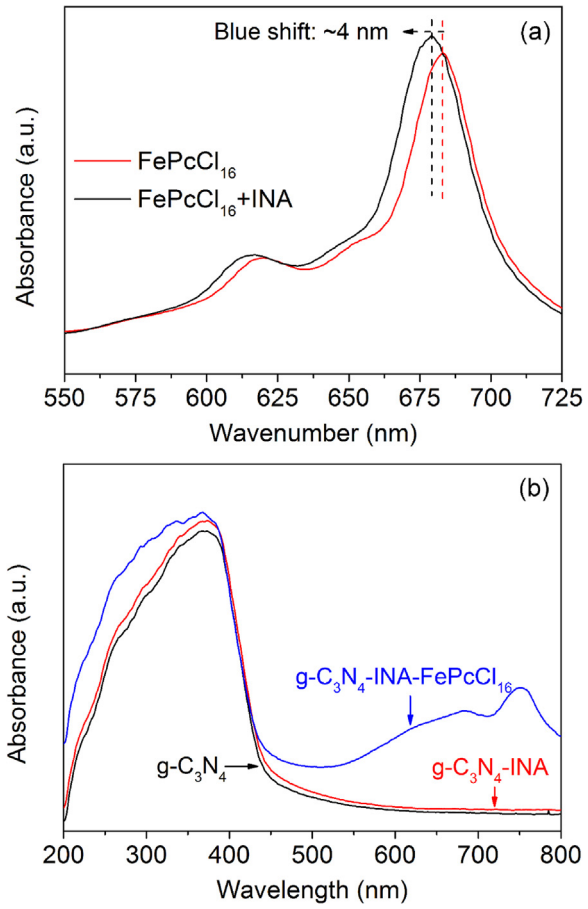

Fig. 1. (a) UV–vis spectra of $FePcCl_{16}$, INA + $FePcCl_{16}$ solution; (b) UV–vis diffuse reflectance absorption spectra of g-C_3N_4, g-C_3N_4-INA and g-C_3N_4-INA-$FePcCl_{16}$.

addition, the as-prepared samples were characterized by FT-IR (see Supplementary material for details).

3.2. Photocatalytic activity

CBZ was selected as the target contaminant to determine the catalytic performance of different catalysts. The impact of $FePcCl_{16}$ loading amount in g-C_3N_4-INA-$FePcCl_{16}$ on the catalytic activity was studied. Fig. 5a shows that, compared with pure g-C_3N_4, the elimination rate of CBZ was higher using g-C_3N_4-INA-$FePcCl_{16}$ with diverse loading amounts of $FePcCl_{16}$ as catalysts. When the actual ratio of $FePcCl_{16}$ reached 1.70%, g-C_3N_4-INA-$FePcCl_{16}$ exhibited the highest photocatalytic activity. The removal rate of CBZ over g-C_3N_4-INA-$FePcCl_{16}$ (3.58%) was lower than g-C_3N_4-INA-$FePcCl_{16}$ (1.70%), possibly because the much amount of $FePcCl_{16}$ in g-C_3N_4-INA-$FePcCl_{16}$ could accelerate the PMS decomposition, and cause quenching after 20 min. As shown in Fig. 5b, PMS was added again after 40 min, which makes the concentration of PMS the same as the initial concentration, and the remaining CBZ was removed completely. This result suggests that the poor photocatalytic activity of g-C_3N_4-INA-$FePcCl_{16}$ (3.58%) is attributed to a lack of PMS. Therefore, in the ensuing studies, g-C_3N_4-INA-$FePcCl_{16}$ (1.70%) was selected to explore the catalytic activity of g-C_3N_4-INA-$FePcCl_{16}$.

As shown in Fig. 6a, nearly 55% CBZ was degraded over g-C_3N_4 or g-C_3N_4/$FePcCl_{16}$ in the presence of PMS under visible light irradiation (λ > 420 nm) within 40 min. In the presence of g-C_3N_4-INA-$FePcCl_{16}$, the removal rate of CBZ reached ~94%, which implies that g-C_3N_4-INA-$FePcCl_{16}$ possesses a higher catalytic oxidation capacity. While $FePcCl_{16}$ shows a poor photocatalytic activity for CBZ degradation, which may be because of the molecular aggregation of $FePcCl_{16}$. The catalytic activity of different catalysts without visible light irradiation was also explored (Fig. 6b). Even though PMS was used, almost no degradation of CBZ occurred when $FePcCl_{16}$, g-C_3N_4 or g-C_3N_4/$FePcCl_{16}$ was present. However, when g-C_3N_4-INA-$FePcCl_{16}$ was present, nearly 49% CBZ was removed, which was greater than that of g-C_3N_4/$FePcCl_{16}$. Based on these results, g-C_3N_4-INA-$FePcCl_{16}$ is considered an efficient activator for PMS, and the enhanced catalytic activity did not result from the sensitization effect, but from the synergistic effect between g-C_3N_4 and $FePcCl_{16}$.

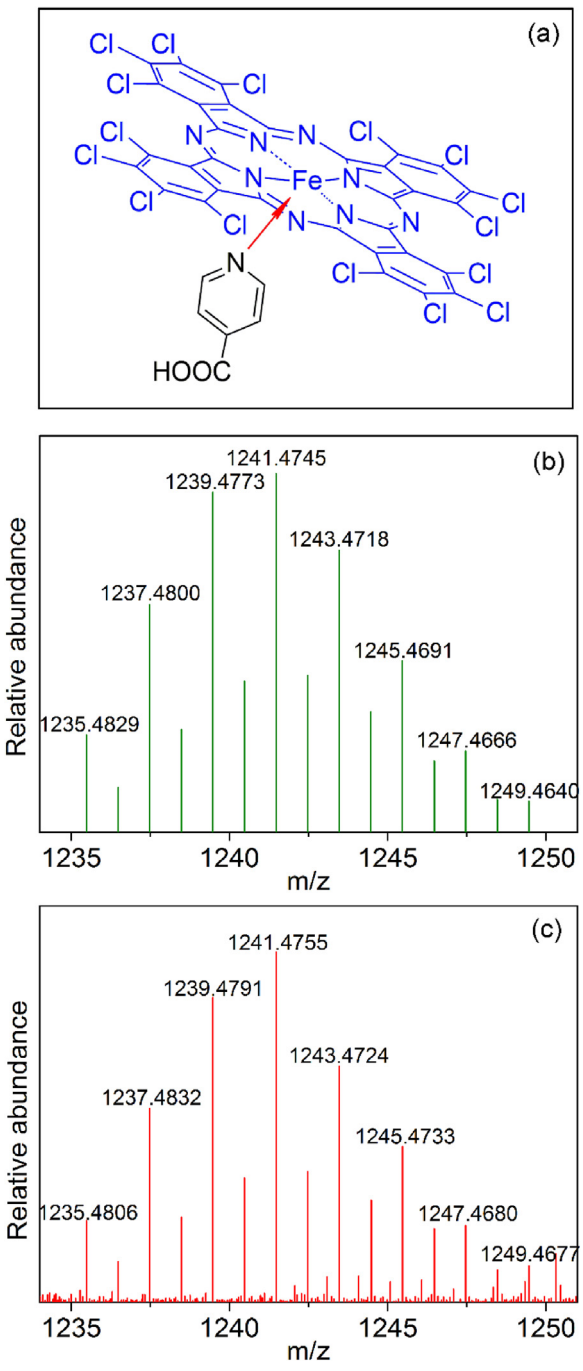

Fig. 2. (a) Molecular structure of INA-$FePcCl_{16}$; (b) Theoretical mass spectrum of INA-$FePcCl_{16}$; (c) The actual mass spectrum of INA and $FePcCl_{16}$ in THF solution.

For the decomposition of organic contaminants in aqueous solution, the pH value is a nonnegligible factor. Efficient catalytic activity commonly occurs within an acidic pH range. Here,

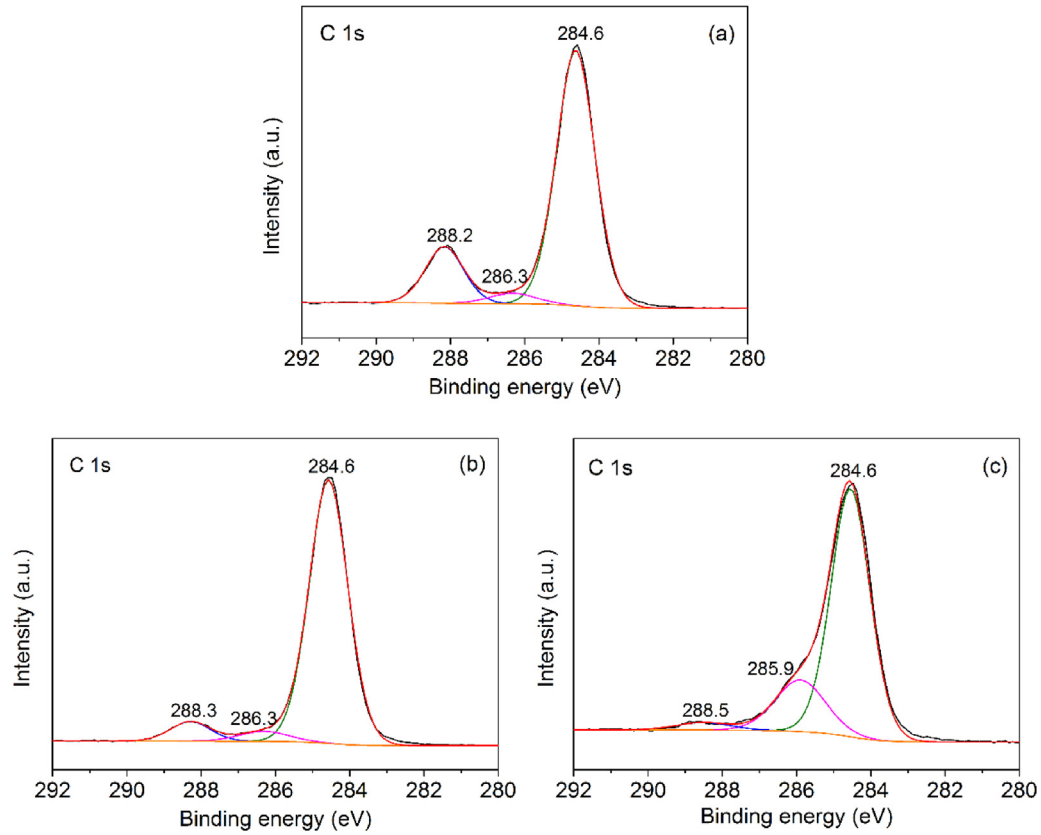

Fig. 3. Curve fit of the C 1s peak of (a) g-C_3N_4, (b) g-C_3N_4-INA-$FePcCl_{16}$, (c) $FePcCl_{16}$.

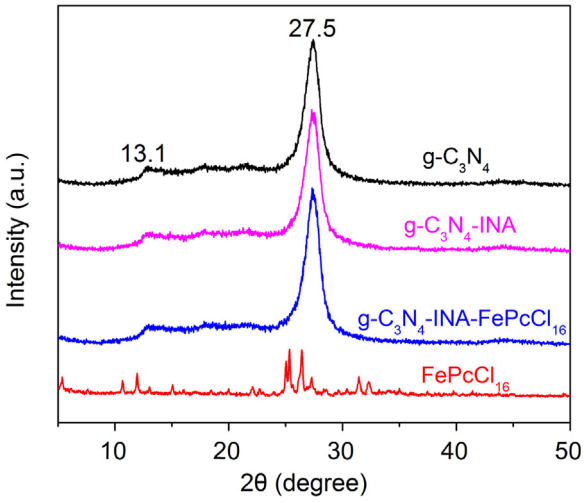

Fig. 4. XRD pattern of g-C_3N_4, g-C_3N_4-INA, g-C_3N_4-INA-$FePcCl_{16}$ and $FePcCl_{16}$.

we investigated the photocatalytic oxidation of CBZ with PMS, g-C_3N_4/PMS and g-C_3N_4-INA-$FePcCl_{16}$/PMS under visible light irradiation under diverse pH conditions. Fig. 7 shows that in the PMS/visible light system, only a small removal of CBZ was observed despite the pH range. The g-C_3N_4/PMS/visible light system showed a good photocatalytic activity under acidic conditions (pH 5), but possessed a relatively weak oxidizing capacity at pH 9. In the g-C_3N_4-INA-$FePcCl_{16}$/PMS/visible light system, the removal rate of CBZ has been maintained around 94% within 40 min at pH 5 and pH 7, and more than 80% at pH 9. The results indicate that g-C_3N_4-INA-$FePcCl_{16}$ exhibited stronger photocatalytic ability over a broader pH range than g-C_3N_4. More importantly, it revealed that the introduction of $FePcCl_{16}$ may lead to a distinctive photocatalytic mechanism that differs from g-C_3N_4. The result is very important to remediate practical wastewater, because wastewater that contains PhACs and other contaminants is typically neutral or alkaline.

The effect of initial PMS concentration was investigated (Fig. S4). With an increase in PMS concentration, the CBZ degradation rate improved gradually. The influence of g-C_3N_4-INA-$FePcCl_{16}$ dosage was also studied (Fig. S5). The removal rate of CBZ was enhanced with increased dosage. However, when the dosage of g-C_3N_4-INA-$FePcCl_{16}$ reached 0.2 g/L, the CBZ degradation was nearly quenched after 20 min, which may have resulted from the rapid decomposition of PMS. This phenomenon is similar to that of g-C_3N_4-INA-$FePcCl_{16}$ (3.58%). Fig. S6 shows the removal rate of CBZ over g-C_3N_4-INA-$FePcCl_{16}$ in the presence of PMS under visible or solar light. The removal of CBZ under solar light only accelerated a little compared with that under visible light irradiation. This indicates that the visible light provides a major contribution to the oxidation process. The degradation of other typical PhACs and organic contaminants is listed in Table S1.

Given that catalyst reusability is a primary concern in practical applications, recycling experiments were conducted with g-C_3N_4-INA-$FePcCl_{16}$/PMS system that was exposed to visible radiation. Fig. S7 shows that, the removal rate of CBZ was as high as 90% over ten reaction cycles, which indicates that g-C_3N_4-INA-$FePcCl_{16}$ presented an excellent reusability. In addition, the fresh and used g-C_3N_4-INA-$FePcCl_{16}$ samples were characterized by XPS to further examine the g-C_3N_4-INA-$FePcCl_{16}$ stability (Fig. S8). The Cl 2p peaks of the used sample show no significant differences from the fresh sample. The results revealed that the g-C_3N_4-INA-$FePcCl_{16}$/PMS/visible light system is a stable and environmentally friendly catalytic oxidation process, and could be used widely.

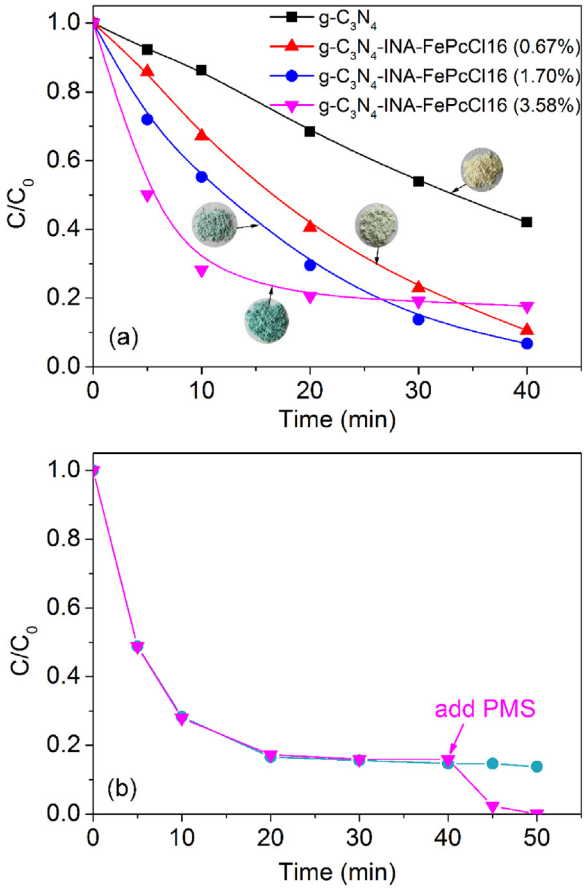

Fig. 5. (a) Photocatalytic degradation of CBZ over g-C_3N_4-INA-$FePcCl_{16}$ with different loading amount in the presence of PMS under visible light irradiation (λ > 420 nm); (b) Photocatalytic degradation of CBZ over g-C_3N_4-INA-$FePcCl_{16}$ (3.58%) in the presence of PMS and adding PMS extra under visible light irradiation (λ > 420 nm). [CBZ] = 25 μM, [g-C_3N_4] = 0.1 g/L, [g-C_3N_4-INA-$FePcCl_{16}$ (0.67%), (1.70%), (3.58%)] = 0.1 g/L, [PMS] = 0.18 mM, pH 7.

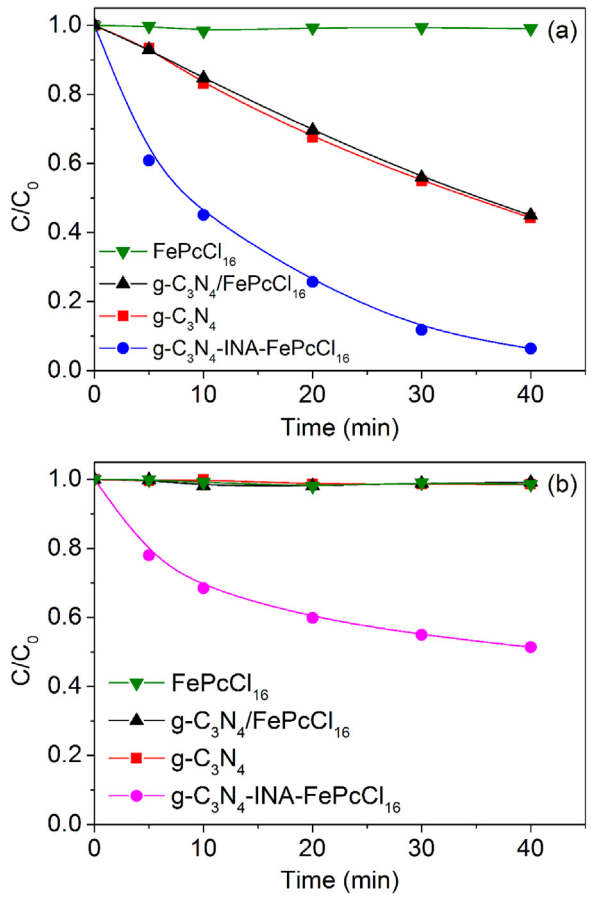

Fig. 6. Degradation of CBZ over $FePcCl_{16}$, g-C_3N_4, g-C_3N_4/$FePcCl_{16}$ and g-C3N_4-INA-$FePcCl_{16}$ in the presence of PMS under different conditions: (a) under visible light irradiation (λ > 420 nm); (b) in the dark. [CBZ] = 25 μM, [g-C_3N_4] = 0.1 g/L, [g-C_3N_4/$FePcCl_{16}$] = 0.1 g/L, [g-C_3N_4-INA-$FePcCl_{16}$] = 0.1 g/L, [PMS] = 0.18 mM, pH 7. (The dosage of $FePcCl_{16}$ is same with its content in g-C_3N_4-INA-$FePcCl_{16}$.).

3.3. Mechanism and pathway

3.3.1. Mechanism

PL is regarded as a potential technology to demonstrate the electron-migration behavior [58,59]. Fig. 8a shows PL spectra of g-C_3N_4 and g-C_3N_4-INA-$FePcCl_{16}$ under the excitation wavelength of 350 nm. Both g-C_3N_4 and g-C_3N_4-INA-$FePcCl_{16}$ exhibited a wide luminescence peak centered at ~450 nm. The g-C_3N_4 has a strong PL emission peak, which implies the fast recombination of photogenerated electron-hole pairs. In contrast with g-C_3N_4, the PL intensity of g-C_3N_4-INA-$FePcCl_{16}$ was reduced visibly, which indicates the existence of the enhanced charge transfer capability between $FePcCl_{16}$ and g-C_3N_4. To further explain the photogenerated electrons migration process, the transient photocurrent response was investigated. Photocurrent-time experiments were carried out through on-off cycles under visible light (λ > 420 nm) irradiation by a 100 W lamp. Fig. 8b shows that g-C_3N_4-INA-$FePcCl_{16}$ exhibited a better response to visible light irradiation than g-C_3N_4, which indicates that the photogenerated electron-hole pairs of g-C_3N_4-INA-$FePcCl_{16}$ are separated efficiently and the recombination rate is lower. However, the photocurrent density response of g-C_3N_4/$FePcCl_{16}$ was slightly weaker than g-C_3N_4. It suggests that the interaction between g-C_3N_4 and $FePcCl_{16}$ via mechanical mixing method is weak, and the introduction of $FePcCl_{16}$ may affect the absorbance of g-C_3N_4. Therefore, it is necessary to combine g-C_3N_4 and $FePcCl_{16}$ via pyridine-based ligand INA.

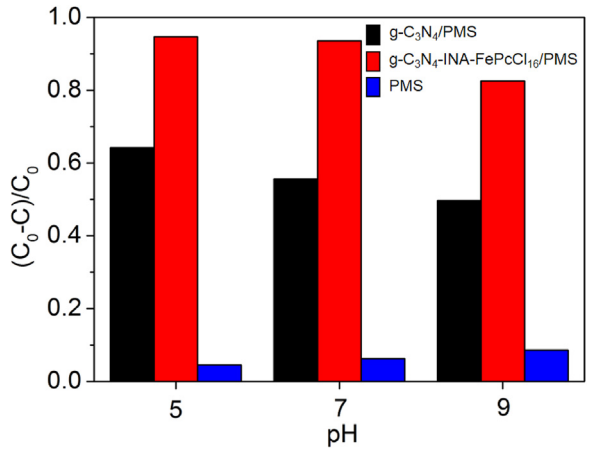

Fig. 7. The removal rate for the photocatalytic degradation of CBZ at different pH values under visible light irradiation (λ > 420 nm) within 40 min. [CBZ] = 25 μM, [g-C_3N_4] = 0.1 g/L, [g-C_3N_4-INA-$FePcCl16$] = 0.1 g/L, [PMS] = 0.18 mM.

In general, the degradation of organic contaminants in the PMS activating process is very likely ascribed to active radicals. Thus, EPR was used to determine the type of active radicals that was involved in the following system where CBZ could be destroyed rapidly: (i) g-C_3N_4-INA-$FePcCl_{16}$/PMS/visible light system; (ii) g-C_3N_4-INA-$FePcCl_{16}$/PMS/dark system; (iii) g-C_3N_4/PMS/visible light system. DMPO was used as the trapping reagent. Fig. 9

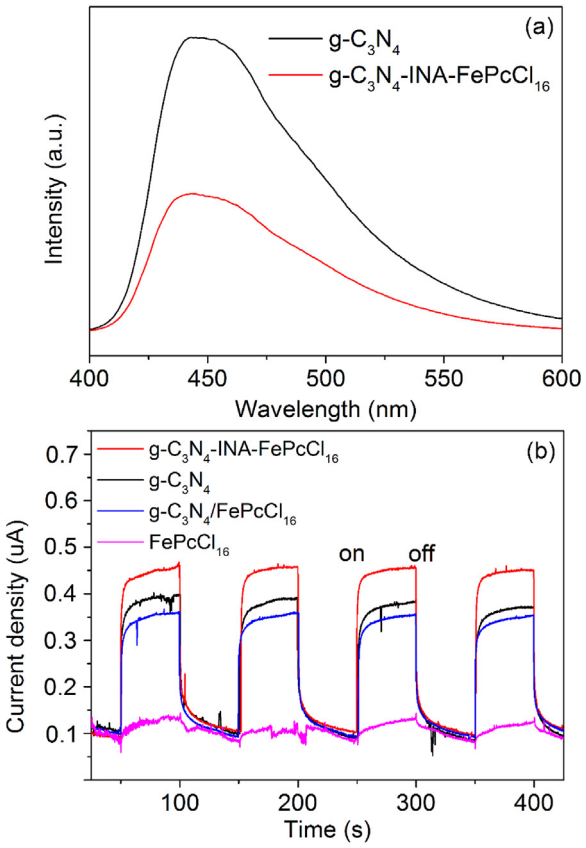

Fig. 8. (a) Photoluminescence (PL) spectra of g-C_3N_4 and g-C_3N_4-INA-$FePcCl_{16}$. (b) The transient photocurrent density response of g-C_3N_4, $FePcCl_{16}$, g-C_3N_4/$FePcCl_{16}$ and g-C_3N_4-INA-$FePcCl_{16}$ photocatalysts electrodes with light on-off cycles under visible light irradiation (λ > 420 nm). [Na_2SO_4] = 0.1 M.

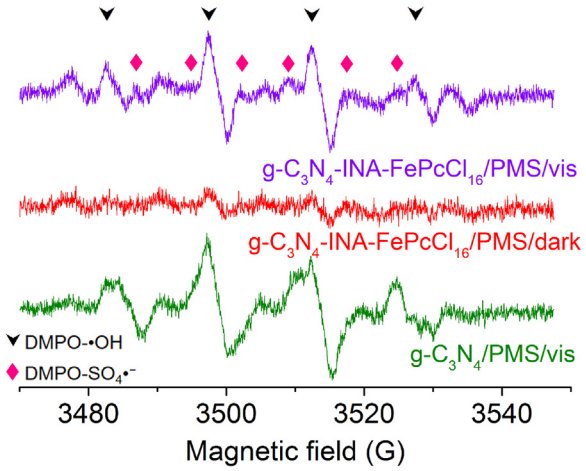

Fig. 9. DMPO spin-trapping EPR spectra in CBZ aqueous solution of different catalytic system. [CBZ] = 25 μM, [g-C_3N_4] = 0.1 g/L, [g-C_3N_4/$FePcCl_{16}$] = 0.1 g/L, [g-C_3N_4-INA-$FePcCl_{16}$] = 0.1 g/L, [PMS] = 0.18 mM, [DMPO] = 50 mM, pH 7.

shows that the EPR spectra of g-C_3N_4-INA-$FePcCl_{16}$/PMS/visible light system and g-C_3N_4/PMS/visible light system showed a four-line and a six-line signal, which were identified as the characteristic peaks of DMPO—•OH and DMPO—SO_4•⁻ adducts. For the g-C_3N_4-INA-$FePcCl_{16}$/PMS/dark system, the peak of the DMPO—•OH and DMPO—SO_4•⁻ signal is visible, but it was weaker. It is worth noting that for the EPR spectra of the g-C_3N_4-INA-$FePcCl_{16}$/PMS/dark system, other small peaks are visible, which may form from the oxidation reaction between g-C_3N_4-INA-$FePcCl_{16}$ and DMPO, which resulted in a relatively weaker DMPO—•OH and DMPO—SO_4•⁻ signal. We conclude that •OH and SO_4•⁻ were generated in three different system, which plays a significant role in removing contaminants.

To investigate other potential active species that are involved in the photocatalytic degradation of CBZ, we conducted designed experiments. Fe (IV) = O species can oxidize sulfoxides (e.g., DMSO, methyl phenyl sulfoxide) into corresponding sulfones through a two-electron transfer step (reaction (1)), which differs from the

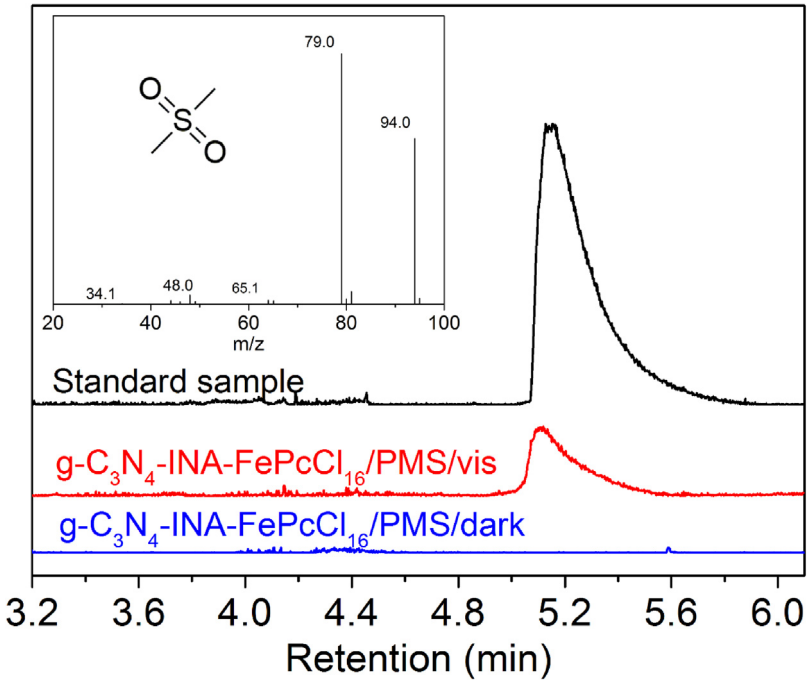

Fig. 10. GC–MS chromatograms of $DMSO_2$ (1 mM), oxidation products of DMSO catalyzed by different catalytic system. The inset shows the MS spectrum of $DMSO_2$.

•OH products (reaction (2)), and the SO_4•$^-$ products are similar to the •OH products [60,61].

$$Fe(IV) = O + (CH_3)_2SO \rightarrow (CH_3)_2SO_2 \quad (1)$$

$$2\text{•}OH + 2(CH_3)_2SO + O_2 \rightarrow 2CH_3SO_2H + HCHO + CH_3OH \quad (2)$$

As shown in Fig. 10, an obvious peak of the standard sample ($DMSO_2$) emerged at ~5.15 min. A peak with similar retention time was detected in the g-C_3N_4-INA-$FePcCl_{16}$/PMS/visible light system. Parallel experiment was carried out in the g-C_3N_4-INA-$FePcCl_{16}$/PMS/dark system, but no $DMSO_2$ signal was observed. Therefore, we can conclude that active Fe (IV) = O species were generated only in the g-C_3N_4-INA-$FePcCl_{16}$/PMS/visible light system.

We summarize that there are •OH, SO_4•$^-$ and Fe (IV) = O species in the g-C_3N_4-INA-$FePcCl_{16}$/PMS/visible light system. To investigate the contribution of these active species to CBZ degradation, quenching tests were carried out with ethanol (EtOH) and tert-butyl alcohol (TBA) as radical scavengers. EtOH can react with both •OH ($K_{\text{•OH/EtOH}}$: $9.1 \times 10^6\ M^{-1}\ s^{-1}$) and SO_4•$^-$ ($K_{SO4\text{•}-/EtOH}$: $3.5 \times 10^7\ M^{-1}\ s^{-1}$), whereas TBA is used mainly to scavenge •OH ($K_{\text{•OH/TBA}}$: $(3.8\text{-}7.6) \times 10^8\ M^{-1}\ s^{-1}$) instead of SO_4•$^-$ ($K_{SO4\text{•}-/TBA}$: $(4.0\text{-}9.1) \times 10^5\ M^{-1}\ s^{-1}$) [62]. We adopted a general pseudo-first order kinetic model $(\ln(C_t/C_0)/k_{obs}t)$ to assess the degradation of CBZ in the presence of different scavengers. As shown in Fig. 11, with an increase in TBA concentration, k_{obs} decreased from 0.067 to 0.038, 0.029 and 0.025 min^{-1} gradually, which indicates that •OH is an important factor in CBZ degradation. For EtOH, the quenching effect was more obvious with a k_{obs} that decreased from 0.067 to 0.017, 0.013 and 0.009 min^{-1}, respectively. This result suggests that SO_4•$^-$ was also generated in the g-C_3N_4/PMS/visible light system. Although 200 mM EtOH was added, the k_{obs} still remained to be 0.009 min^{-1}, which was considered to result from the contribution of Fe (IV) = O species. Therefore, we infer that •OH, SO_4•$^-$ and Fe (IV) = O play an equal role in the degradation in the g-C_3N_4-INA-$FePcCl_{16}$/PMS/visible light system. Quenching tests were also carried out in the g-C_3N_4-INA-$FePcCl_{16}$/PMS/dark system (Fig. S9). When 10 mM TBA and EtOH were added, the CBZ removal

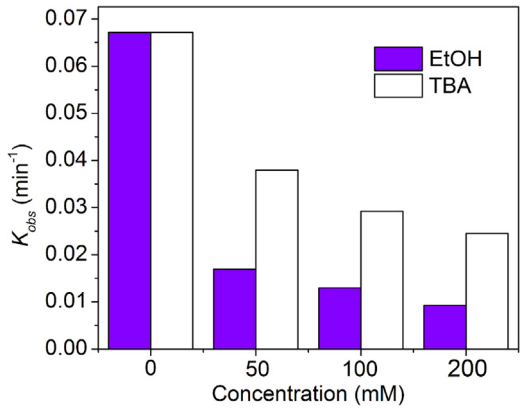

Fig. 11. Effects of different concentration of ethanol (EtOH) and tert-butyl alcohol (TBA) on CBZ removal over g-C_3N_4-INA-$FePcCl_{16}$ in the presence of PMS under visible light irradiation (λ > 420 nm) within 40 min. [CBZ] = 25 μM, [g-C_3N_4-INA-$FePcCl_{16}$] = 0.1 g/L, [PMS] = 0.18 mM, pH 7.

rate dropped from 49% to 45% and 35%, respectively. The result confirms that SO_4•$^-$ and •OH were involved in the g-C_3N_4-INA-$FePcCl_{16}$/PMS/dark system, which was consistent with the EPR analysis.

According to the aforementioned conclusion and related reports, a proposed photocatalytic mechanism for activation of PMS over g-C_3N_4-INA-$FePcCl_{16}$ is shown in Fig. 12. The g-C_3N_4 and $FePcCl_{16}$ can be excited under visible light irradiation, and the photogenerated electrons of g-C_3N_4 itself and those that migrated from the *$FePcCl_{16}$ can be captured by PMS to produce SO_4•$^-$, which can react with OH^- to gain •OH [63]. Photogenerated holes of g-C_3N_4 could react with PMS to generate SO_5•$^-$, which possesses a lower oxidizing capacity [38]. On the other hand, the *Fe^{II} ions of *$FePcCl_{16}$ coordinated with the O atom of PMS for the cleavage of the O—O bond. Active Fe (IV) = O species was produced via heterolysis of the O—O bond, and simultaneous homolysis occurred to

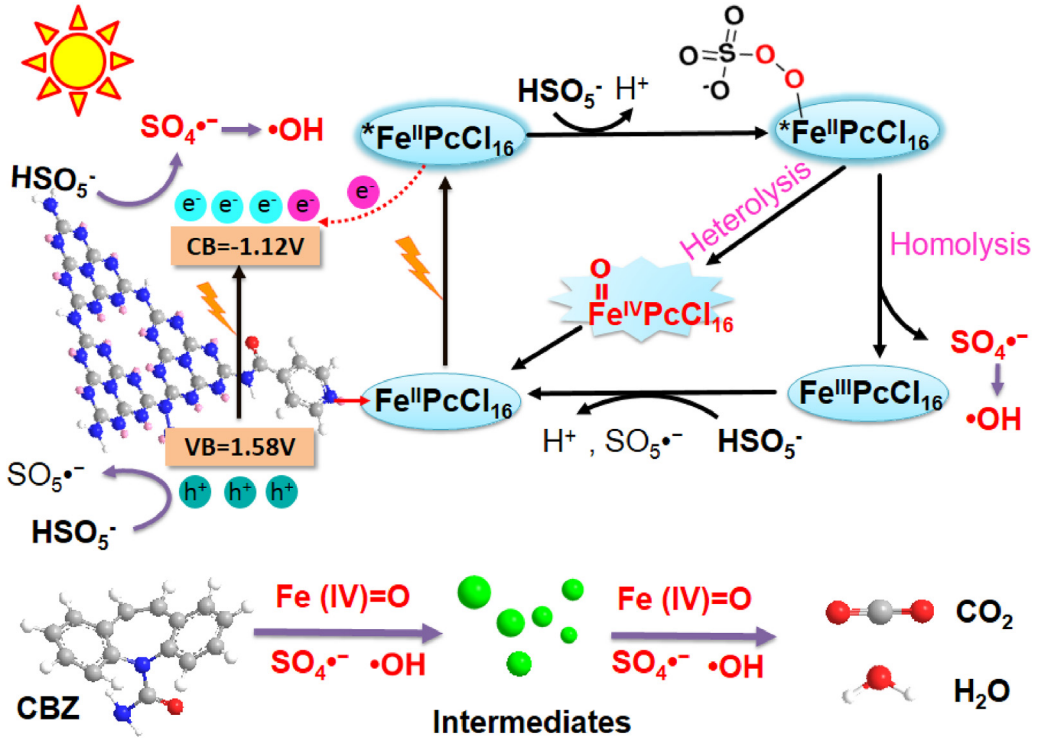

Fig. 12. The proposed mechanism for the CBZ degradation over g-C_3N_4-INA-$FePcCl_{16}$ in the presence of PMS under visible light irradiation (λ > 420 nm).

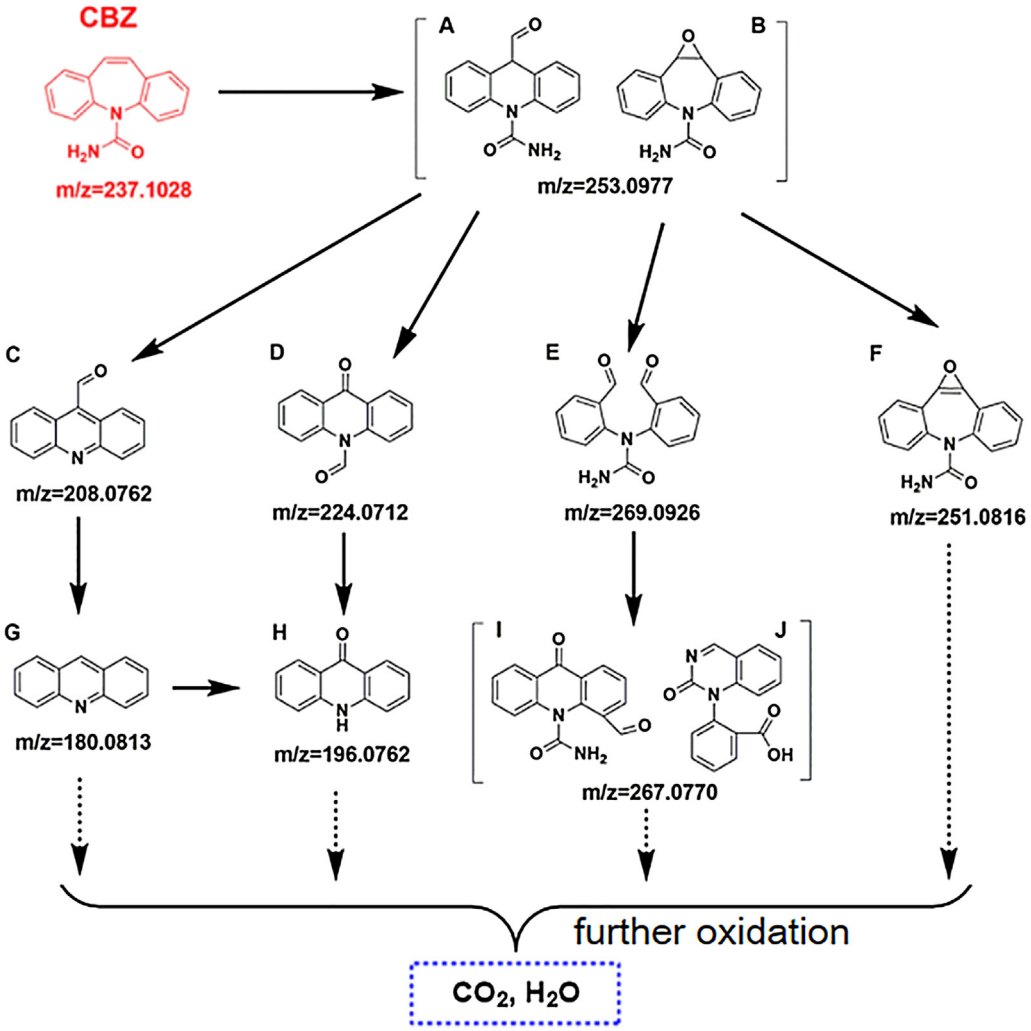

Scheme 2. Possible pathway for the photocatalytic degradation of CBZ over g-C_3N_4-INA-$FePcCl_{16}$ in the presence of PMS under visible light irradiation (λ > 420 nm).

generate $SO_4^{\bullet-}$ and •OH. Active species of Fe (IV) = O, $SO_4^{\bullet-}$ and •OH oxidize CBZ in the g-C_3N_4-INA-$FePcCl_{16}$/PMS/visible light system. Moreover, the mechanism for the g-C_3N_4-INA-$FePcCl_{16}$/PMS/dark system was also proposed (Fig. S10). Without visible light irradiation, only $FePcCl_{16}$ could contribute to the removal of CBZ, $SO_4^{\bullet-}$ and •OH radicals were generated only through O—O bond homolysis, whereas heterolysis hardly occurred because no Fe (IV) = O species were detected in the dark condition.

3.3.2. CBZ degradation pathway

In the process of identifying the degradation pathway of CBZ, ten intermediates (A–J) were detected by HDMS in positive ion mode. Details of different intermediates are listed in Table S2. We proposed a possible degradation pathway of CBZ (Scheme 2). Compounds A and B with the same formula $C_{15}H_{13}N_2O_2$, are attributed to the initial products of CBZ, which contain one more oxygen atom than the CBZ molecule. Compound A, followed by the loss of $-CONH_2$ group, lead to the formation of C. Compound D may form by B via a facile ring contraction [64], and compounds E and F were other further oxidation products of compounds A or B owing to the attack of •OH, $SO_4^{\bullet-}$ or Fe (IV) = O species. Compound H could result from D through the removal of a carbonyl group, or be formed by further oxidation of G. Compounds I and J could originate from E by intramolecular cyclization and intramolecular attack, respectively [65]. In addition, the mineralization of CBZ by PMS can be expressed by reaction (3) [66].

$$C_{15}H_{12}N_2O + 82HSO_5^- \rightarrow 15CO_2 + 47H_2O + 2NO_3^- + 82SO_4^{2-} \quad (3)$$

According to reaction 3, 1 mol CBZ requires 82 mol PMS for complete mineralization. In our investigated condition, the complete mineralization of the added CBZ (25 μM) will consume 2.05 mM PMS. As shown in Table S3, all intermediates remained after 40 min in the presence of 0.18 mM PMS. Considering the experimental conditions and mineralization, 0.18 mM PMS was added every 40 min. After 11 times intervals, when the total PMS addition was close to the amount of complete mineralization, all intermediates disappeared. In light of our preceding strategy for the determination of final products, GC–MS combined with HDMS was used, but no small molecular acids were detected. We infer that all the intermediates would be mineralized to CO_2 and H_2O with sufficient PMS.

4. Conclusion

In summary, a novel photocatalyst g-C_3N_4-INA-$FePcCl_{16}$ was prepared to activate PMS for the rapid removal of refractory contaminants. The enhanced catalytic oxidation activity of g-C_3N_4-INA-$FePcCl_{16}$ could be attributed to a perfect coordination interaction between functionalized g-C_3N_4 and $FePcCl_{16}$, which extended the spectral response region of g-C_3N_4 and improved the dispersibility of $FePcCl_{16}$, and benefited electron migration from

$FePcCl_{16}$ to g-C_3N_4. These advantages facilitated the effective formation of Fe (IV)=O, $SO_4^{\bullet-}$ and •OH species for CBZ removal. $^*FePcCl_{16}$ was identified as key role in accelerating the generation of Fe (IV)=O. This mechanism was different from most reported PMS activation processes, where •OH and $SO_4^{\bullet-}$ are recognized as the dominant active species. Furthermore, the g-C_3N_4-INA-$FePcCl_{16}$/PMS/visible light system exhibited a wide pH tolerance and good reusability. This work provides a new perspective for combining different catalysts via an axial coordination route, and provides a new photocatalytic system for the wastewater treatment, which is conducive to sustainable environmental development.

Author contributions

The manuscript was written through contributions of all authors. All authors have given approval to the final version of the manuscript.

Notes

The authors declare no competing financial interest.

Acknowledgments

This work was supported by the National Natural Science Foundation of China (No. 51133006), and Zhejiang Provincial Natural Science Foundation of China (No. LY14E030013 and LQ17E030003), and the Public Welfare Technology Application Research Project of Zhejiang Province (NO. 2015C33018).

Appendix A. Supplementary data

Supplementary data associated with this article can be found, in the online version, at http://dx.doi.org/10.1016/j.apcatb.2017.06.057.

References

[1] D. Bendz, N.A. Paxéus, T.R. Ginn, F.J. Loge, J. Hazard. Mater. 122 (2005) 195.
[2] D.P. Mohapatra, S.K. Brar, R.D. Tyagi, P. Picard, R.Y. Surampalli, Sci. Total Environ. 470–471 (2014) 58–75.
[3] M.J. Focazio, D.W. Kolpin, K.K. Barnes, E.T. Furlong, M.T. Meyer, S.D. Zaugg, L.B. Barber, M.E. Thurman, Sci. Total Environ. 402 (2008) 201–216.
[4] Y. Ren, L. Lin, J. Ma, J. Yang, J. Feng, Z. Fan, Appl. Catal. B: Environ. 165 (2015) 572–578.
[5] A.H. Mady, M.L. Baynosa, D. Tuma, J.-J. Shim, Appl. Catal. B: Environ. 203 (2017) 416–427.
[6] M.A. Fontecha-Cámara, C. Moreno-Castilla, M.V. López-Ramón, M.A. Álvarez, Appl. Catal. B: Environ. 196 (2016) 207–215.
[7] Y.H. Guan, J. Ma, Y.M. Ren, Y.L. Liu, J.Y. Xiao, L.Q. Lin, C. Zhang, Water Res. 47 (2013) 5431–5438.
[8] X. Li, Z. Wang, B. Zhang, A.I. Rykov, M.A. Ahmed, J. Wang, Appl. Catal. B: Environ. 181 (2016) 788–799.
[9] G.P. Anipsitakis, D.D. Dionysiou, Environ. Sci. Technol. 37 (2003) 4790–4797.
[10] Y. Ding, L. Zhu, N. Wang, H. Tang, Appl. Catal. B: Environ. 129 (2013) 153–162.
[11] E. Saputra, S. Muhammad, H. Sun, H.-M. Ang, M.O. Tade, S. Wang, Appl. Catal. B: Environ. 142 (2013) 729–735.
[12] Y. Feng, D. Wu, Y. Deng, T. Zhang, K. Shih, Environ. Sci. Technol. 50 (2016).
[13] Y.H. Guan, J. Ma, X.C. Li, J.Y. Fang, L.W. Chen, Environ. Sci. Technol. 45 (2011) 9308–9314.
[14] S. Su, W. Guo, C. Yi, Y. Leng, Z. Ma, Ultrason. Sonochem. 19 (2012) 469–474.
[15] H. Sun, C.K. Kwan, A. Suvorova, H.M. Ang, M.O. Tadé, S. Wang, Appl. Catal. B: Environ. 154–155 (2014) 134–141.
[16] C. Wang, J. Kang, H.Q. Sun, H.M. Ang, M.O. Tade, S.B. Wang, Carbon 102 (2016) 279–287.
[17] Y. Feng, D. Wu, Y. Deng, T. Zhang, K. Shih, Environ. Sci. Technol. 50 (2016) 3119–3127.
[18] H. Zhang, Z. Wang, C. Liu, Y. Guo, N. Shan, C. Meng, L. Sun, Chem. Eng. J. 250 (2014) 76–82.
[19] A. Rastogi, S.R. Alabed, D.D. Dionysiou, Water Res. 43 (2009) 684–694.
[20] F. Gong, L. Wang, D. Li, F. Zhou, Y. Yao, W. Lu, S. Huang, W. Chen, Chem. Eng. J. 267 (2015) 102–110.
[21] H. Lin, J. Wu, H. Zhang, Chem. Eng. J. 244 (2014) 514–521.
[22] J. Zou, J. Ma, L. Chen, X. Li, Y. Guan, P. Xie, C. Pan, Environ. Sci. Technol. 47 (2013) 11685.
[23] A. Sorokin, J.L. Seris, B. Meunier, Science 26 (1995) 1163–1166.
[24] D. Dai, Z. Yang, Y. Yao, L. Chen, G. Jia, L. Luo, Catal. Sci. Technol. 7 (2017) 934–942.
[25] X. Zhang, T. Peng, L. Yu, R. Li, Q. Li, Z. Li, ACS Catal. 5 (2015) 504–510.
[26] L. Zhang, W. Wang, S. Sun, Y. Sun, E. Gao, J. Xu, Appl. Catal. B: Environ. 132–133 (2013) 315–320.
[27] A. Hamdi, S. Boufi, S. Bouattour, Appl. Surf. Sci. 339 (2015) 128–136.
[28] X. Tao, W. Ma, T. Zhang, J. Zhao, Angew. Chem. 40 (2001) 3014–3016.
[29] Q. Wang, H. Li, J.-H. Yang, Q. Sun, Q. Li, J. Yang, Appl. Catal. B: Environ. 192 (2016) 182–192.
[30] P. Fita, T. Osmalek, T. Goslinski, M. Wierzchowski, J. Mielcarek, J. Photochem. Photobiol. A: Chem. 232 (2012) 44–49.
[31] J. Hu, H. Liu, L. Wang, N. Li, T. Xu, W. Lu, Z. Zhu, W. Chen, Carbon 100 (2016) 408–416.
[32] R. Baker, D.P. Wilkinson, J. Zhang, Electrochim. Acta 54 (2009) 3098–3102.
[33] H. Liu, S. Bao, Z. Cai, T. Xu, N. Li, L. Wang, H. Chen, W. Lu, W. Chen, Chem. Eng. J. 317 (2017) 1092–1098.
[34] A. Thomas, A. Fischer, F. Goettmann, M. Antonietti, J.O. Muller, R. Schlogl, J.M. Carlsson, J. Mater. Chem. 18 (2008) 4893–4908.
[35] S. Shi, M.A. Gondal, A.A. Al-Saadi, R. Fajgar, J. Kupcik, X. Chang, K. Shen, Q. Xu, Z.S. Seddigi, J. Colloid Interface Sci. 416 (2014) 212–219.
[36] F. Dong, Z. Zhao, T. Xiong, Z. Ni, W. Zhang, Y. Sun, W.K. Ho, ACS Appl. Mater. Interfaces 5 (2013) 11392–11401.
[37] X. Li, Y. Pi, L. Wu, Q. Xia, J. Wu, Z. Li, J. Xiao, Appl. Catal. B: Environ. 202 (2017) 653–663.
[38] Y. Tao, Q. Ni, M. Wei, D. Xia, X. Li, A. Xu, RSC Adv. 5 (2015) 44128–44136.
[39] H. Dong, M. Wei, J. Li, J. Fang, L. Gao, X. Li, A. Xu, RSC Adv. 6 (2016) 70747–70755.
[40] M. Wei, L. Gao, J. Li, J. Fang, W. Cai, X. Li, A. Xu, J. Hazard. Mater. 316 (2016) 60–68.
[41] L. Zhang, X. Chen, J. Guan, Y. Jiang, T. Hou, X. Mu, Mater. Res. Bull. 48 (2013) 3485–3491.
[42] X. Ma, Y. Lv, J. Xu, Y. Liu, R. Zhang, Y. Zhu, Phys. Chem. C 116 (2012) 23485–23493.
[43] H. Liu, D. Chen, Z. Wang, H. Jing, R. Zhang, Appl. Catal. B: Environ. 203 (2017) 300–313.
[44] Y. Hong, Y. Jiang, C. Li, W. Fan, X. Yan, M. Yan, W. Shi, Appl. Catal. B: Environ. 180 (2016) 663–673.
[45] S. Min, G. Lu, J. Phys. Chem. C 116 (2012) 19644–19652.
[46] Q. Liang, M. Zhang, C. Liu, S. Xu, Z. Li, Appl. Catal. A: Gen. 519 (2016) 107–115.
[47] L. Yu, X. Zhang, C. Zhuang, L. Lin, R. Li, T. Peng, Phys. Chem. Chem. Phys. 16 (2014) 4106–4114.
[48] W. Lu, T. Xu, Y. Wang, H. Hu, N. Li, X. Jiang, W. Chen, Appl. Catal. B: Environ. 180 (2016) 20–28.
[49] X. Chen, W. Lu, T. Xu, N. Li, D. Qin, Z. Zhu, G. Wang, W. Chen, Appl. Catal. B: Environ. 201 (2017) 518–526.
[50] J. Metz, O. Schneider, M. Hanack, Inorg. Chem. 23 (1984) 1065–1071.
[51] X. Zhang, X. Xie, H. Wang, J. Zhang, B. Pan, Y. Xie, J. Am. Chem. Soc. 135 (2013) 18–21.
[52] S. Zhang, L. Zhao, M. Zeng, J. Li, J. Xu, X. Wang, Catal. Today 224 (2014) 114–121.
[53] J. Li, B. Shen, Z. Hong, B. Lin, B. Gao, Y. Chen, Chem. Commun. 48 (2012) 12017–12019.
[54] A. Thomas, A. Fischer, F. Goettmann, M. Antonietti, J.-O. Müller, R. Schlögl, J.M. Carlsson, J. Mater. Chem. 18 (2008) 4893.
[55] K. Nilson, P. Palmgren, J. Åhlund, J. Schiessling, E. Göthelid, N. Mårtensson, C. Puglia, M. Göthelid, Surf. Sci. 602 (2008) 452–459.
[56] J. Zhang, M. Zhang, G. Zhang, X. Wang, ACS Catal. 2 (2012) 940–948.
[57] Y. Wang, J. Yao, H. Li, D. Su, M. Antonietti, J. Am. Chem. Soc. 133 (2011) 2362–2365.
[58] Z. Li, Y. Wu, G. Lu, Appl. Catal. B: Environ. 188 (2016) 56–64.
[59] A. Habibi-Yangjeh, A. Akhundi, J. Mol. Catal. A: Chem. 415 (2016) 122–130.
[60] S.-Y. Pang, J. Jiang, J. Ma, Environ. Sci. Technol. 45 (2011) 3179–3180.
[61] C. Tai, J.-F. Peng, J.-F. Liu, G.-B. Jiang, H. Zou, Anal. Chim. Acta 527 (2004) 73–80.
[62] F. Qi, W. Chu, B. Xu, Appl. Catal. B: Environ. 134–135 (2013) 324–332.
[63] L.J. Xu, W. Chu, L. Gan, Chem. Eng. J. 263 (2015) 435–443.
[64] Z. Zhu, Y. Chen, Y. Gu, F. Wu, W. Lu, T. Xu, W. Chen, Water Res. 93 (2016) 296–305.
[65] Y.F. Rao, W. Chu, Y.R. Wang, Appl. Catal. A: Gen. 468 (2013) 240–249.
[66] Y. Ding, H. Tang, S. Zhang, S. Wang, H. Tang, J. Hazard. Mater. 317 (2016) 686–694.